ELSEVIER

Journal of Fluids and Structures 25 (2009) 42–59

JOURNAL OF FLUIDS AND STRUCTURES

www.elsevier.com/locate/jfs

Flow-excited acoustic resonances of coaxial side-branches in an annular duct

D. Arthurs, S. Ziada*

Department of Mechanical Engineering, McMaster University, Hamilton, ON, Canada L8S 4L8

Received 14 December 2006; accepted 16 March 2008
Available online 22 May 2008

Abstract

This paper investigates the aeroacoustic response of an annular duct with closed coaxial side-branches, and examines the effect of several passive countermeasures on the resonance intensity. The investigated geometry is inspired by the design of the Roll-Posts in the Rolls-Royce LiftSystem® engine, which is currently being developed for the Lockheed Martin Joint Strike Fighter (JSF®) aircraft. The effects of design parameters, such as diameter ratio, branch length ratio and thickness of the annular flow on the frequency and resonance intensity of the first acoustic mode are studied experimentally. Numerical simulations of the acoustic mode shapes and frequencies are also performed. The annular flow has been found to excite several acoustic modes, the strongest in all cases being the first acoustic mode, which consists of a quarter wavelength along the length of each branch. The ratios of the branch length and diameter, with respect to the main duct diameter, have been found to have strong effects on the frequency of the acoustic modes.

Keywords: Acoustic resonance; Coaxial side-branch; Annular duct

1. Introduction

Problems involving acoustic resonance in piping systems with closed side-branches are common in industrial applications and have been reported by several authors such as Chen and Florjancic (1975), Chen and Stürchler (1977), Baldwin and Simmons (1986) and Gillessen and Roller (1989). Generally, the flow in the main pipe excites a standing sound wave consisting of an odd number of quarter wavelengths along the length of each branch in single and coaxial side-branch systems, as illustrated in Fig. 1.

This phenomenon often generates large pressure oscillations in the side-branches and may result in severe noise and/or vibration problems and possibly fatigue failure of the piping system or its associated instrumentations. Previous investigations of this phenomenon by Bruggeman et al. (1991), Ziada and Bühlmann (1992) and Ziada (1993), among others, have shown that the pulsation amplitude in the side-branches can be much higher than the dynamic head in the main pipe. This phenomenon can therefore pose serious limitations on the reliable operation of piping systems with closed side-branches. A recent example of the damaging effects of this phenomenon is the acoustic fatigue damage of the steam dryer of a boiling water reactor in Quad Cities nuclear plant. In this case, the pressure pulsations generated by

*Corresponding author.
E-mail address: ziadas@mcmaster.ca (S. Ziada).

0889-9746/$ - see front matter
doi:10.1016/j.jfluidstructs.2008.03.007

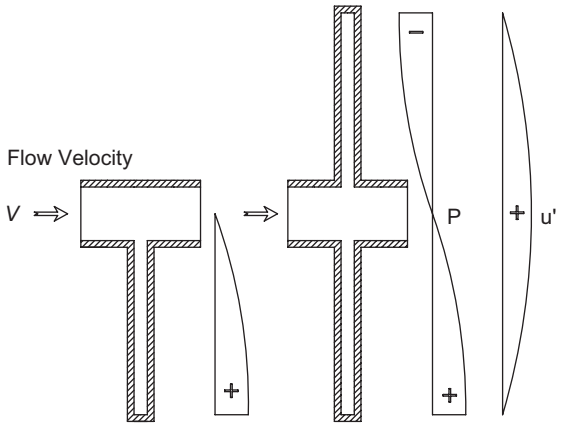

Fig. 1. First acoustic mode consisting of $\frac{1}{4}$ wavelength along each branch for the case of single and coaxial side-branches. P and u' are the acoustic pressure and particle velocity, respectively.

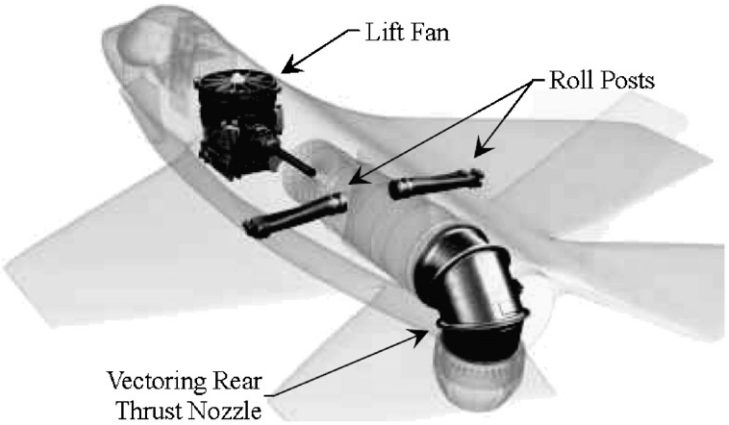

Fig. 2. Rolls-Royce vertical Liftsystem® showing engine and roll post configuration of the joint strike fighter. (http://www.rolls-royce.com/defence_aerospace/products/combat/liftsystem/default.jsp).

acoustic resonance in the standpipes of safety relief valves propagated upstream in the main steam pipeline and acoustically loaded the steam dryer (Deboo et al., 2007; NRC Information Notice 2002-26, 2002).

Flow-excited acoustic resonance of closed side-branches is caused by a feedback mechanism between the instability of the free shear layer at the mouth of the branch and the acoustic particle velocity generated by the branch's resonant modes. It has been shown by Michalke (1965) that instabilities in the shear layer are unstable relative to disturbances for a range of frequencies. The acoustic particle velocity provided by the acoustic standing wave has been shown by Ziada (1994) to provide such disturbances, thereby establishing a feedback mechanism where one phenomenon reinforces the other.

The sound power $\Pi(t)$ generated at any instant by vorticity convection in a sound field has been formulated by Howe (1975), and it is given by

$$\Pi(t) = -\rho \int \boldsymbol{\omega} \cdot (\mathbf{v} \times \mathbf{u})\, d\forall, \tag{1}$$

where ρ is the fluid density, $\boldsymbol{\omega}$ is the vorticity, $\mathbf{v}$ is the fluid velocity, $\mathbf{u}$ the particle velocity of the sound field and $\forall$ is the volume containing the vorticity field. When this relation is integrated over one complete acoustic cycle, it will result in the net acoustic power being either generated or lost within the volume of integration, $\forall$. A positive net acoustic power indicates that the oscillations can be self-sustaining.

Systems with closed side-branches are susceptible to this type of excitation because the vorticity field, $\boldsymbol{\omega}$, associated with the shear layer is coincident with the location of the maximum acoustic particle velocity, $\mathbf{u}$, which is a favourable

condition to maximize the power integral in Eq. (1). In particular, well-tuned coaxial branches have very small acoustic losses and are therefore capable of generating very intense acoustic resonances over wide ranges of flow velocity. This has been demonstrated by Graf and Ziada (1992), who found that only 2% of the coaxial branches acoustic power is radiated into the main pipe.

Acoustic resonance of coaxial side-branches is the topic of this paper. However, the branches in the present case are connected to an annular duct, which is different from all previous investigations. Investigation of this pipe configuration is inspired from the Roll-Post design of the vertical lift system of the Joint Strike Fighter (JSF®), which is schematically illustrated in Fig. 2. During the normal (forward) flight mode, the Roll-Posts are closed at their outlets and are exposed to low Mach number flow at their inlets, which are connected to the by-pass annular duct of the engine. Under these flight conditions, the Roll-Posts approximate closed coaxial side-branches exposed to a grazing annular flow. This paper investigates the effect of design parameters on the aeroacoustic response of such a system. The effect of some passive counter-measures on the resonance intensity is also examined.

2. Experimental approach

2.1. Experimental set-up

All experiments and numerical simulations were performed in the aeroacoustic laboratory at McMaster University. A test geometry reflecting the main features of the JSF® Roll-Post and engine geometry was constructed using PVC. Tests were performed with air at atmospheric pressure and room temperature. The test-section was positioned at the inlet side of a centrifugal blower powered by a 50 HP induction motor and controlled by a variable frequency drive. Figs. 3 and 4 show the experimental set-up and the main geometrical parameters for the test-section.

Using this arrangement, it was possible to perform tests at flow velocities in the main duct up to approximately $V = 110$ m/s. This was sufficient to excite the lowest three acoustic modes of the branches. As shown in Fig. 3, a parabolic contraction was used at the test-section inlet to provide a uniform flow with a thin boundary layer. A conical diffuser with an included angle of 14° was attached to the test-section outlet and the diffuser outlet was connected to the blower by means of a flexible duct. The flexible duct was used to isolate the test-section from any vibrations produced by the blower/motor assembly.

The main duct of the test-section had an inner diameter of $D = 152$ mm and an overall length of $L_o = 355$ mm with the coaxial side-branches being approximately centred along its length. The diameter of the side-branches was fixed at $d = 38$ mm; however, the length of the branches was adjustable using a set of movable plugs. The plugs were sealed in the branches using an o-ring to prevent any acoustic leakage. Microphones were flush mounted in the plugs to measure the pressure pulsation within the two side-branches.

Fig. 3. Experimental set-up showing the inlet contraction and test-section.

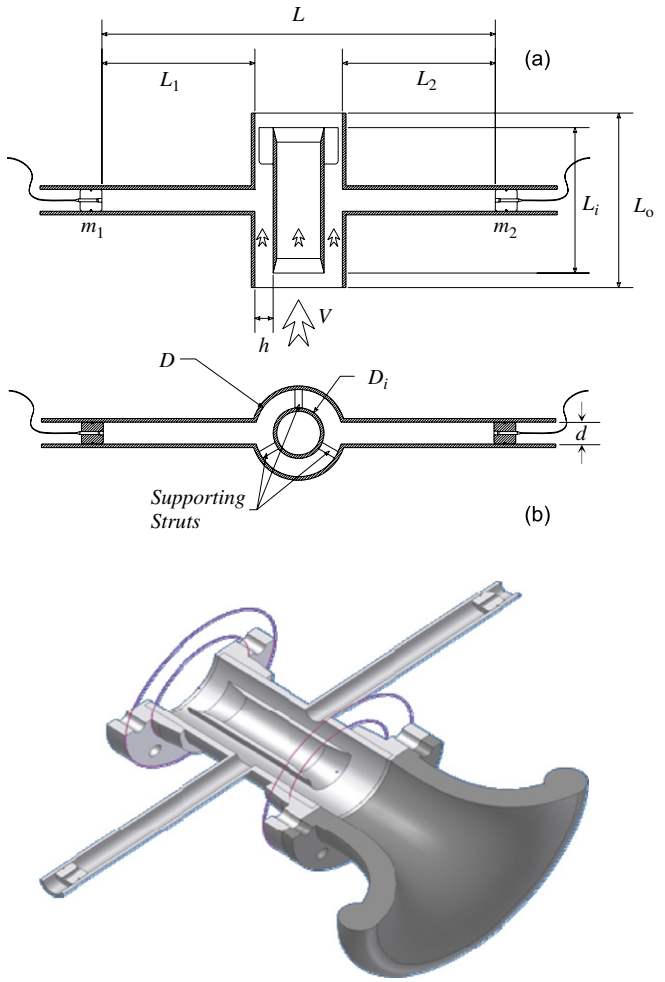

Fig. 4. Geometry of test-section showing (a) the inner cylinder, supporting struts and microphone locations m_1 and m_2 and (b) a three-dimensional view.

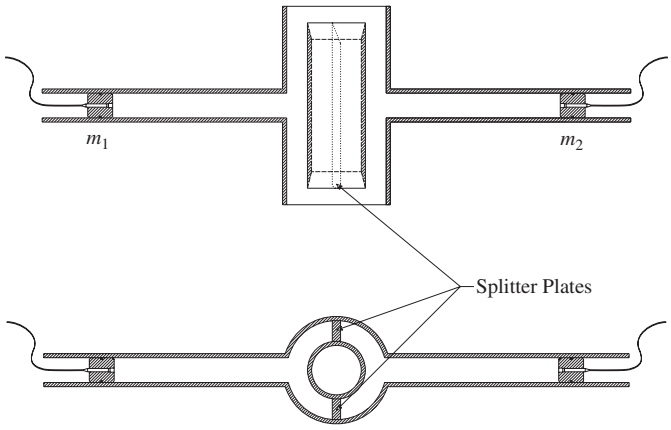

Fig. 5. Splitter plate design.

All concentric, inner cylinders, which were used to form the annular duct, had a fixed length of $L_i = 254$ mm and were centered with respect to the outer duct. Various sizes of inner cylinders were constructed and used to test the effect of the annular gap thickness, h. The inner cylinder was attached to the outer one by means of three supporting struts located downstream of the side-branches, as shown in Fig. 4. The leading edges of the struts were rounded, and all other edges beveled at 30° to minimize the effects of vortex shedding from leading and trailing edges. These features are shown in Fig. 4.

Two splitter plates were constructed and tested to evaluate their effectiveness as a passive countermeasure. As shown in Fig. 5, the splitter plates were positioned vertically in the annular gap to divide the annular duct into two halves along the entire length of the inner cylinder ($L_i = 254$ mm). The plates extended from the outer diameter of the inner cylinder to the inner diameter of the main duct. All joining surfaces were well sealed using rubber gaskets to ensure no acoustic leakage was present. The leading edges of the splitter plates were rounded and the trailing edges were beveled at 30° to alleviate vortex shedding from these edges.

Data were collected by two condenser microphones attached to the movable plugs located at the end of each side-branch. The data were captured by a National Instruments BNC 2140 data acquisition board and analyzed by means of LabView software, which computed the frequency spectra for each channel and the phase between the two microphones. The data were acquired in 20 sets of 1 s samples at a sampling rate of 16 384 Hz.

2.2. Numerical simulation of acoustic modes

To better understand the acoustic mode shapes encountered during physical testing, the tested geometry was modeled using Abaqus® FEA software. A 4-node tetrahedral mesh was used to construct numerical models for all tested geometries. A sample model showing the mesh is shown in Fig. 6. The boundary conditions at each end of the duct were set to zero acoustic pressure to simulate the open ended duct, with all other surfaces being modeled as solid boundaries with a zero pressure gradient. The finite element simulation solves the Helmholtz equation in three dimensions for the control volume and outputs all mathematically possible eigenvalues for that volume. The effects of flow are not considered in the solver as these simulations were used only to predict acoustic frequencies and mode shapes.

The resulting pressure distribution for each eigenvalue is a three-dimensional representation of the corresponding acoustic mode. It should be noted that the numerical simulation yields every mathematically possible eigenvalue for the acoustic modes. However, only those with an acoustic pressure node located in the main duct, resulting in small acoustic radiation losses, were excited during the experiments. The results of the numerical simulations have been compared with those obtained from experiments. It was possible to identify the acoustic modes observed in the experiments from the measured frequency of the oscillation and the phase shift between the pressure oscillations at the closed ends of the two side-branches. In the following sections, the experimental results, together with the numerical simulations of the first three acoustic modes, which were observed during experiments, are presented.

Table 1 shows the results from the numerical simulations in comparison to frequencies measured during testing. For all cases, including those presented below, the numerical simulations showed excellent accuracy and were within 2% of measured values. In addition, Bravo et al. (2004) reported an accuracy of less than 2% using finite element analysis to predict resonance frequencies and mode shapes.

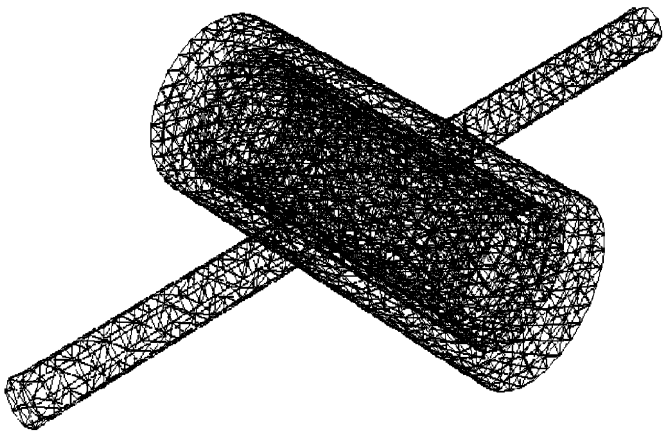

Fig. 6. Sample of 4-node tetrahedral mesh used for acoustic mode simulation.

Table 1
Simulated and measured frequencies of the first three acoustic modes of the system

	$f_{numerical}$ (Hz)	f_{actual} (Hz)
1st mode	298.8	304
2nd mode	862.6	859
3rd mode	953.1	951

2.3. Dimensionless parameters

The main results in this paper are presented in the form of dimensionless pressure, which is the root mean square amplitude of acoustic pressure, P_{rms}, normalized by the dynamic head in the main (annular) pipe according to the relation:

$$P^* = \frac{P_{rms}}{\frac{1}{2}\rho V^2}, \tag{2}$$

where ρ is the density of the fluid in the duct, and V is the flow velocity in the main duct. These pressure amplitudes are plotted against the reduced velocity, V_r, which is given by

$$V_r = \frac{V}{f_1 d}, \tag{3}$$

where f_1 is the frequency of the first acoustic mode and d is the side-branch diameter.

3. Overview of aeroacoustic response

Acoustic resonances within the duct were excited almost continuously for a range of flow velocities in the main pipe from 17 to 112 m/s. As an example of the acoustic response of the duct, the test results of the baseline geometry, with $h/d = 1.0$, are discussed in some detail. Fig. 7 shows the frequency and amplitude of the dominant component in the pressure spectra measured at the closed ends of the side-branches. As the flow velocity is increased, three acoustic modes, labelled f_1 through f_3, are excited consecutively. As illustrated in Fig. 7(a), the Strouhal number, fd/V, at which these modes are excited remains in the range 0.26–0.56, which agrees well with the range reported by Ziada and Shine (1999) for coaxial branches.

Resonance of mode f_1, the lowest mode observed during testing, was initiated at a flow velocity in the duct near 21 m/s and continued until approximately 50 m/s. The frequency of this mode was ~304 Hz, and its amplitude was the highest of all the acoustic modes encountered during testing, reaching a value of 5300 Pa or 168.5 dB. This acoustic mode was identified by means of the numerical simulation in conjunction with its measured frequency and an observed phase shift of 180° between the pressure oscillations at the two closed ends of the branches. As shown in Fig. 8, it consists of one-half an acoustic wavelength (λ) between the closed ends of the side-branches. The acoustic pressure node is therefore placed in the main annular duct, which minimizes the acoustic pressure in the main duct and the resulting acoustic radiation from the side-branches into the main duct. A typical acoustic pressure spectrum measured at the end of one branch and a flow velocity of 40 m/s is also shown in Fig. 8. The dominance of the resonating first mode is apparent. As many as five higher harmonic components ($2f_1$ to $6f_1$) can be observed in the spectrum, which is indicative of nonlinear effects due to high-intensity acoustic resonance at the first mode.

Mode f_2, shown in Fig. 9, the second acoustic mode encountered during testing, had a frequency of ~859 Hz and was excited over a range of flow velocities from 59 to 77 m/s. This mode is structured similarly to mode f_1, with the acoustic pressures at the ends of the branches being 180° out of phase with each other, but involving $3\lambda/2$ between the ends of the two branches. These characteristics can be seen from the numerical simulation results, which show the acoustic pressure distribution for mode f_2. The predicted frequency from the simulation is 862.6 Hz, which agrees well with the measured value of 859 Hz. The amplitude of mode f_2 reached 158 dB, which is quite significant but still smaller than the maximum amplitude produced by mode f_1. This is because of the higher radiation losses for mode f_2 due to its shorter wavelength and the resulting higher acoustic pressure in the main duct. A typical acoustic pressure spectrum taken at 72 m/s whilst mode f_2 was excited is shown in Fig. 9.

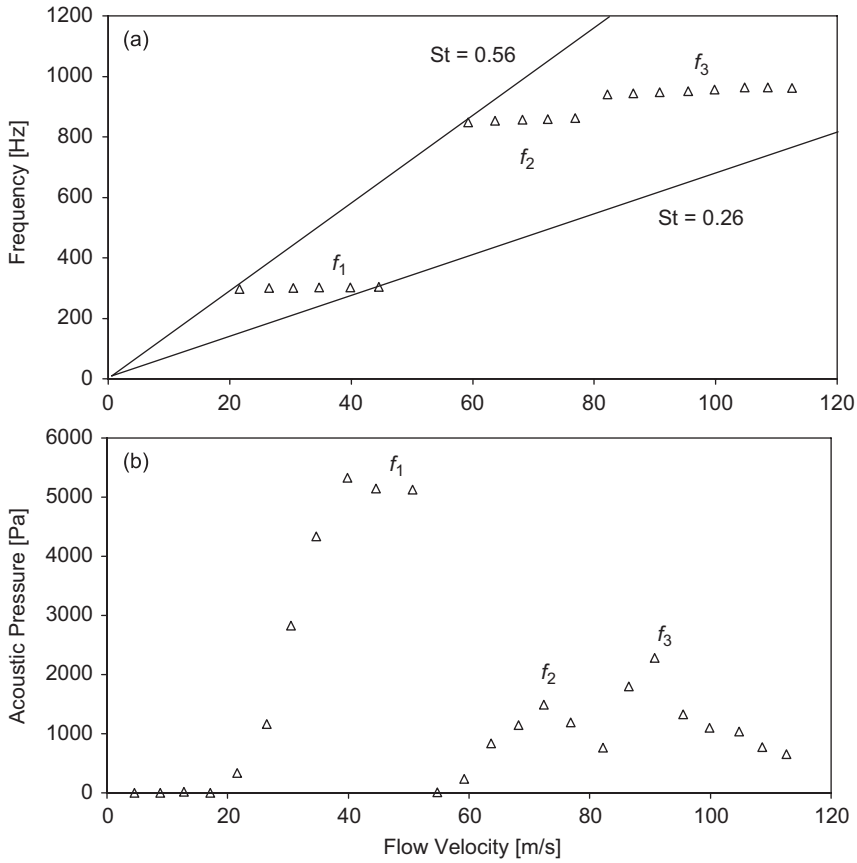

Fig. 7. Overview of the system acoustic response: (a) acoustic resonance (lock-in) frequency and (b) acoustic pressure as functions of flow velocity; $h/d = 1.0$.

Modes f_1 and f_2 are particularly liable to excitation for a number of reasons pertaining to the location of the acoustic pressure node. The position of the acoustic pressure node in the annular duct minimizes the acoustic radiation losses from the branches into the main duct, and thereby allows the generated acoustic energy to be "trapped" in the side-branches. In addition, the position of the node in the centre of the main duct corresponds to the location of maximum acoustic pressure gradient, and thus potentially large acoustic particle velocity. In this case, the maximum acoustic particle velocity occurs near the mouth of the branch, which is the location of the free shear layer over the side-branch mouth. The spatial coincidence of maximum particle velocity and shear layer results not only in effective excitation of the shear layer, but also in efficient generation of acoustic power according to Eq. (1).

Mode f_3, the third acoustic mode excited during the experiments, occurred over a range of flow velocity, 82–112 m/s, at a frequency of 951 Hz. The frequency of this acoustic mode is close to that of mode f_2 discussed earlier, however, the acoustic pressure at the ends of the two side-branches for this mode are in phase with each other. These characteristics can be seen in Fig. 10, which shows the acoustic pressure distribution as obtained from the numerical simulation. The simulation yielded a frequency of 953.1 Hz, which is close to the measured value. A typical frequency spectrum taken at a flow velocity of 91 m/s while Mode f_3 was resonating is depicted in Fig. 10.

Frequency spectra for a range of flow velocities from 0 to 110 m/s were combined to produce the contour plot of sound pressure level (SPL) in dB (re: 20 μPa) for varying flow velocities and frequencies. Fig. 11 shows this contour plot for the baseline case with $h/d = 1.0$. The successive excitation of acoustic modes can be clearly seen. For almost any flow velocity above 20 m/s in the main duct, there is at least one acoustic mode in resonance. This underlines the susceptibility of this duct arrangement to flow-excited acoustic resonance.

We can see that for flow velocities greater than 100 m/s, a fourth acoustic mode of the duct is excited at approximately 1500 Hz. This mode was present for a variety of configurations at high flow rates. However, this mode is

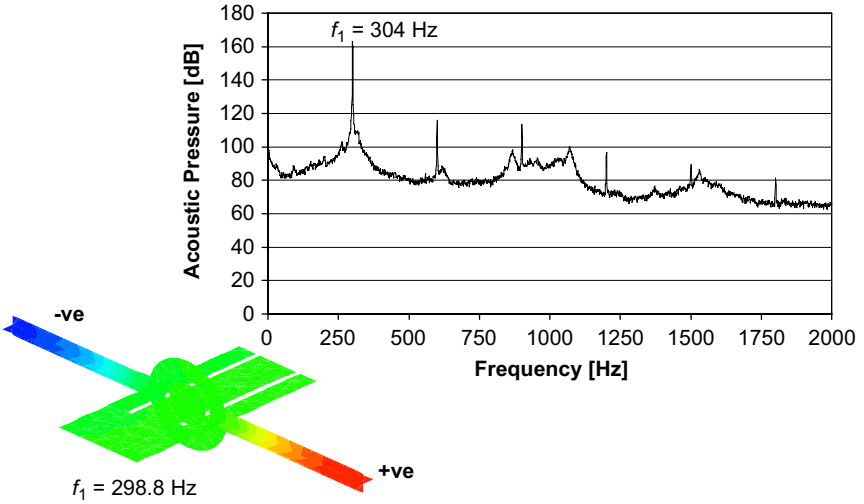

Fig. 8. Frequency spectrum and mode shape for acoustic mode f_1.

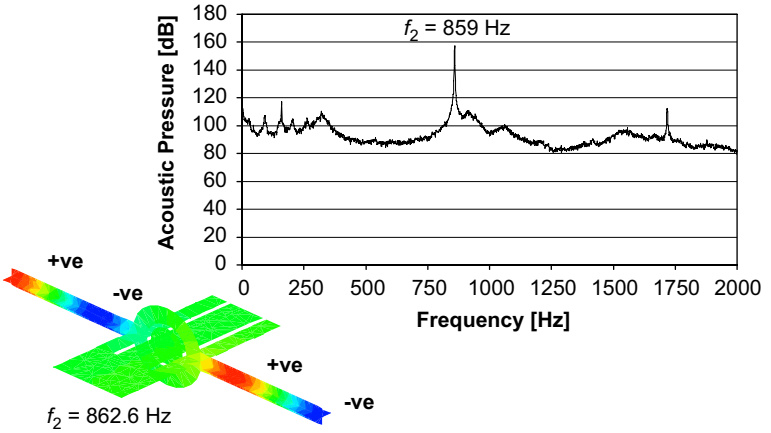

Fig. 9. Frequency spectrum and mode shape for acoustic mode f_2.

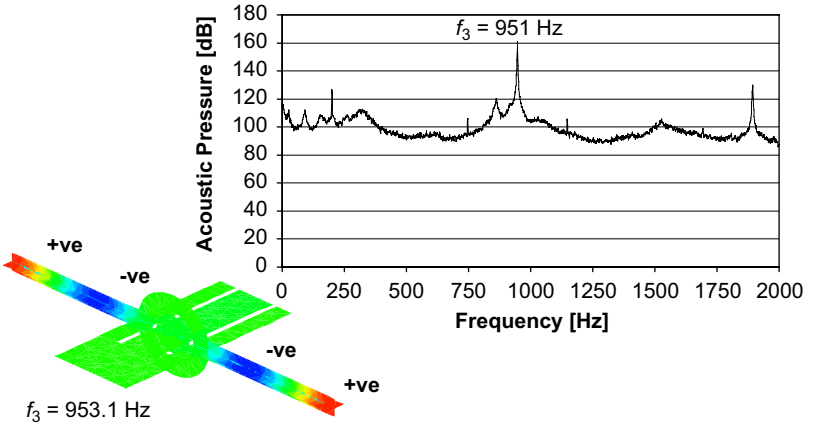

Fig. 10. Frequency spectrum and mode shape for acoustic mode f_3.

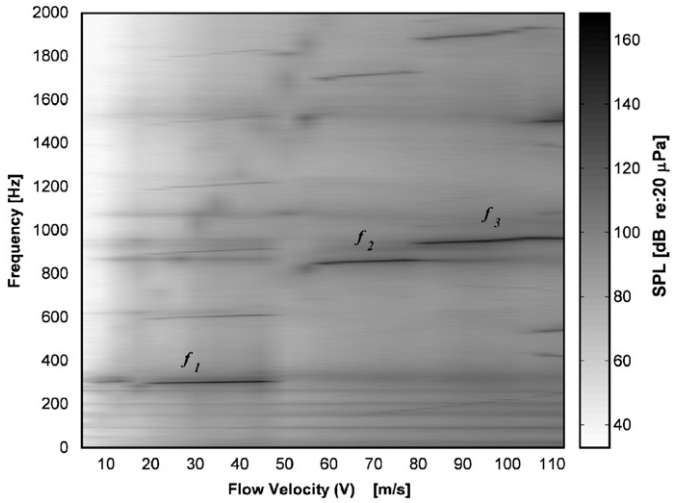

Fig. 11. Sound pressure level in dB for the duct in the baseline configuration; $h/d = 1.0$.

not discussed here in detail because it is excited at flow velocities, which are substantially above those encountered in the JSF® application.

4. Frequencies of the acoustic modes

It has been demonstrated in the literature, such as Ziada and Shine (1999) and Graf and Ziada (1992), that for piping systems with long side-branches ($L_{1,2}/D \gg 1$) and large diameter ratios ($d/D \approx 1.0$), the resonance frequencies of the coaxial side-branch modes can be accurately predicted based on the length between the ends of the side-branches and the speed of sound. The piping system in question here, however, has relatively short and small diameter side-branches ($L_{1,2}/D \approx 1.75$ and $d/D = 0.25$). Using the standard relationship used for long coaxial branches

$$f_{\lambda/2} = \frac{C(2n-1)}{2L}, \tag{4}$$

where L is the *total length* of the side-branches including the diameter of the main duct ($L_1 + L_2 + D$) and n is the acoustic mode number, the frequency predicted for the first acoustic mode of the current geometry is 250 Hz, whereas the actual frequency measured during testing was approximately 304 Hz, a difference of nearly 18%.

The difference between the measured and the predicted frequencies for the first acoustic mode seemed to depend strongly on the branch dimensions relative to the main pipe diameter. To investigate the effect of branch length to branch diameter ratio on the first acoustic mode of the system, a numerical study was performed using the previously discussed finite element techniques. The parameters studied included the ratio of branch length to the main diameter ($L_{1,2}/D$) as well as the ratio between the branch to main pipe diameters (d/D). Fig. 4 shows all geometric parameters for the piping system being investigated. For this study, the inner diameter of the main duct (D) remained constant, while the branch diameter and length were scaled relative to it. The results are shown in Table 2 and Figs. 12 and 13.

Simulations performed with varying sizes of inner cylinders as well as without an inner cylinder showed no significant difference in the frequencies generated for the lower modes. Both the relative branch length ($L_{1,2}/D$) as well as the relative branch diameter (d/D) displayed a strong effect on the frequency of the first mode. The predictions of Eq. (4) deviate from the finite element results by as much as 38% for short branches with small diameter ratios, as seen in Fig. 12.

As the branch diameter was gradually decreased (decreasing d/D), the frequency of the first mode increased. This result can be explained by the increasing effect of the acoustic end correction on each side-branch. As the ratio of d/D is decreased from $d/D = 1$ to 0.25 for a constant branch length ($L_{1,2}$), the end correction becomes a smaller fraction of the effective acoustic length of the pipe, thus decreasing the wavelength of the $\frac{1}{4}$ standing acoustic wave, and the frequency

Table 2
Effect of length and diameter ratios ($L_{1,2}/D$, d/D) on the accuracy of predicting the frequency of the first acoustic mode

	d/D	$f_{\lambda/2}$ (Hz)	$f_{\text{numerical}}$ (Hz)	% Error	f_{single} (Hz)	% Error
$L_{1,2}/D = 10$	1.00	53.59	54.92	2.49	54.10	−1.50
	0.75	53.59	55.24	3.08	54.63	−1.10
	0.50	53.59	55.77	4.07	55.16	−1.09
	0.25	53.59	56.25	4.96	55.71	−0.96
$L_{1,2}/D = 5$	1.00	102.30	106.00	3.61	104.20	−1.70
	0.75	102.30	107.62	5.20	106.16	−1.36
	0.50	102.30	109.43	6.97	108.20	−1.12
	0.25	102.30	111.63	9.12	110.33	−1.16
$L_{1,2}/D = 2$	1.00	225.07	240.25	6.75	234.44	−2.42
	0.75	225.07	247.81	10.11	244.64	−1.28
	0.50	225.07	258.62	14.91	255.76	−1.11
	0.25	225.07	271.60	20.68	267.94	−1.35
$L_{1,2}/D = 1$	1.00	375.11	414.55	10.51	401.90	−3.05
	0.75	375.11	437.44	16.62	432.82	−1.06
	0.50	375.11	469.72	25.22	468.89	−0.18
	0.25	375.11	515.39	37.40	511.51	−0.75

$f_{\lambda/2}$ is the frequency predicted from Eq. (4); f_{single} is predicted from Eq. (5); $f_{\text{numerical}}$ is the predicted frequency from the FEA model.

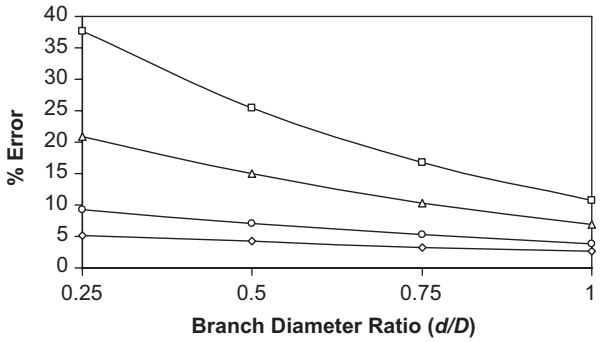

Fig. 12. Percent error of Eq. (4) in predicting the frequency of the first acoustic mode: □, $L_{1,2}/D = 1$; △, $L_{1,2}/D = 2$; ○, $L_{1,2}/D = 5$; ◇, $L_{1,2}/D = 10$.

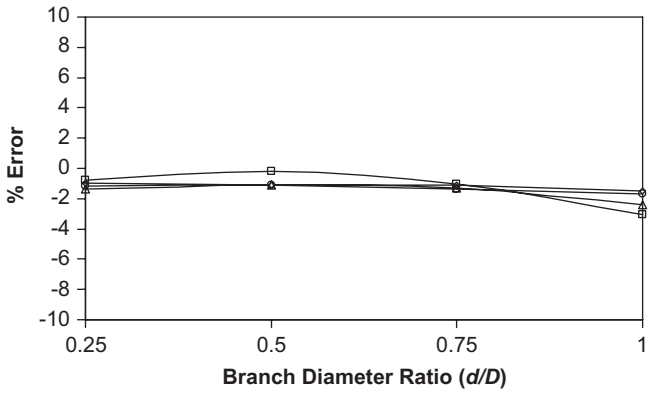

Fig. 13. Percent error of Eq. (5) in predicting the frequency of the first acoustic mode: □, $L_{1,2}/D = 1$; △, $L_{1,2}/D = 2$; ○, $L_{1,2}/D = 5$; ◇, $L_{1,2}/D = 10$.

of the tone is increased. This fact is most apparent for relatively short branch pipes ($L_{1,2}/D = 1$) where the acoustic end correction represents a significant portion of the effective branch length. On the other hand, the frequency $f_{\lambda/2}$ predicted from Eq. (4) does not show any dependence on the diameter ratio, d/D.

The same trend was observed when changing the ratio of $L_{1,2}/D$. As the lengths of the branches were decreased with respect to the main duct diameter, the frequency of the first acoustic mode increased, as one would expect. However, for relatively short branches ($L_{1,2}/D < 2$), the frequency of the first mode is not well predicted by Eq. (4).

The above results suggest that as the diameter ratio d/D is decreased, each branch responds more independently and therefore the resonance frequency may be more accurately determined by considering each branch separately. The resonance frequency of a single side-branch can be obtained from

$$f_{\text{single}} = \frac{C(2n-1)}{4(L_{1,2} + 0.4\,d)}, \tag{5}$$

where $L_{1,2}$ are the individual branch lengths, d is the branch diameter, C is the speed of sound and n is the acoustic mode number. The coefficient $0.4d$ in Eq. (5) represents the acoustic end correction at the open end of the branch (Kinsler et al., 2000).

Table 2 compares the percent errors of Eqs. (4) and (5) for all cases examined in the numerical simulations. It is interesting to note that even for relatively long branches with branch diameter ratios (d/D) of 1, the prediction of frequency using a decoupled single side-branch is more accurate in predicting frequency of the first acoustic mode.

During testing, a first mode frequency of 304 Hz was measured for a branch length $L_{1,2}$ of 266 mm with a main annular duct diameter of 154 mm and a branch diameter of 38 mm. Eq. (4) predicts a frequency of 249.7 Hz, which deviates by 18% from the measured value. Eq. (5) however predicts a frequency of 304.1 Hz with a difference of less than 0.1%. This surprisingly small error in the prediction of Eq. (5) is depicted in Fig. 13 for the tested range of $L_{1,2}/D$ and d/D.

5. Effect of detuning the branches

The effect of offsetting the length of one branch to detune the resonance frequency of one branch from the other was examined both experimentally and numerically. In this case, if the branches were to remain acoustically coupled, i.e. they possess the same resonance frequency, the lack of symmetry would shift the acoustic pressure node away from the main duct and thereby would increase acoustic radiation and reduce the resonance intensity. This technique of altering the length of one or both of the branches has been demonstrated by Ziada and Bühlmann (1992) and Graf and Ziada (1992) to be a very effective attenuation technique for closed side-branches with large diameter ratios (i.e. large d/D).

In the present experiments, one branch was shortened by an amount ΔL in increments of half the branch diameter, $d/2$, and a complete set of frequency spectra for flow velocities up to 110 m/s were obtained. The data are presented hereafter for various values of offset ratio, $\Delta L/L_{1,2}$, where $L_{1,2}$ is the original length of each of the branches, which continued to be the length of the longer branch in all experiments with branch offset.

For branch offsets as small as $\Delta L/L_{1,2} = 7\%$, the appearance of two distinct frequencies f_1' and f_1'' was evident. These two frequencies can be clearly seen in Fig. 14 which shows typical pressure spectra taken from each branch at $\Delta L/L_{1,2} = 42\%$ for a flow velocity in the main duct of $V = 30.5$ m/s. These frequencies corresponded to the resonance frequencies of each of the separate branches and agreed well with those predicted by the acoustic model of Eq. (5) and also with the prediction of the numerical simulation, assuming decoupled, single side-branches. The two distinct frequencies in each of the branches were often observed at the same flow velocity for offset ratios less than $\Delta L/L_{1,2} = 42\%$. Fig. 14(c) shows the magnitude of the two acoustic tones, f_1' and f_1'', as a function of the flow velocity in the main duct for a branch offset ratio of $\Delta L/L_{1,2} = 42\%$. It is evident that the two tones are excited over two different ranges of flow velocity, with the lower frequency tone f_1' being excited for lower flow velocities, and the higher frequency tone f_1'' being excited for higher flow velocities. It was also evident from the frequency spectra as well as the time signals of the two microphones that these two resonant tones were generated simultaneously throughout the range of offset ratio tested, with the lower frequency f_1' tone being produced in the longer unchanged branch at an approximately constant frequency (~310 Hz), and the higher frequency f_1'' tone taking place in the shortened branch.

In addition to the above observations, the two branches displayed very distinct acoustic response over the range of flow velocities tested. Figs. 15 and 16 show the overall acoustic response of the branches in the form of contour plots of the SPL measured by the microphones located at the ends of the branches. Fig. 15, which shows the response of the unchanged branch for the case $\Delta L/L_{1,2} = 42\%$, indicates substantially reduced amplitude of pressure fluctuations for

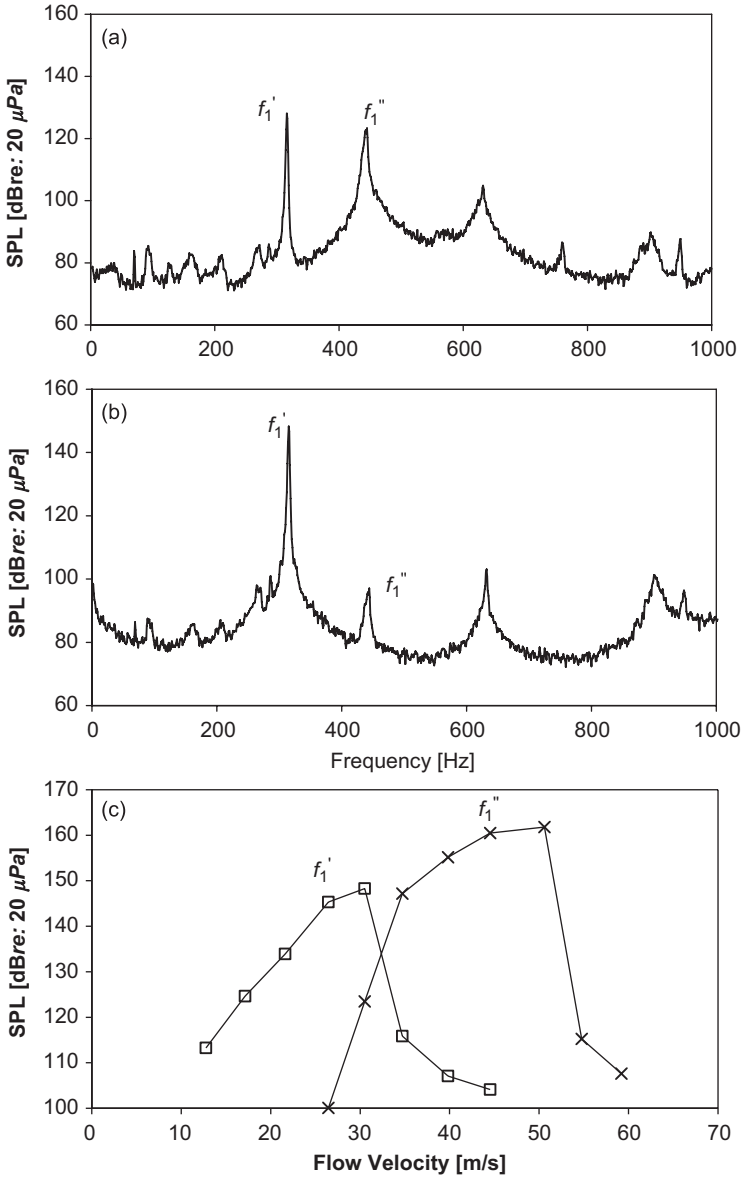

Fig. 14. Frequency spectra of (a) the shortened and (b) unchanged branches for $V = 30.5$ m/s, $\Delta L/L_{1,2} = 42\%$. (c) □, Peak acoustic excitation of f_1' in the unchanged branch ×, f_1'' in the shortened branch; for △, $L/L_{1,2} = 42\%$.

the first acoustic mode near 310 Hz for a range of flow velocities between 20 and 40 m/s. For the shortened branch, however, Fig. 16 clearly illustrates the larger amplitudes associated with the first mode of the shortened branch, which occurs at a higher frequency near 478 Hz. The lock-in also occurs at higher velocities from 30 to 55 m/s because of the higher resonance frequency. The maximum acoustic pressure generated in the shorter branch by this mode is five times larger than that in the unmodified longer branch, and nearly 50% of the acoustic pressure observed in the case *without* branch offset ($\Delta L/L_{1,2} = 0\%$). When these results are presented in a dimensionless format as illustrated in Fig. 17, the first mode resonance is seen to start at virtually the same reduced velocity in all cases, which is in agreement with the study by Ziada and Shine (1999). Moreover, despite the reduction in the resonance intensity due to detuning, the pressure pulsation amplitude is still excessive, reaching twice the dynamic head for the shorter branch. From a practical point of view, the usage of Roll-Posts with offset in their lengths is obviously undesirable, especially when this offset must be large to produce sufficient reduction in the resonance intensity.

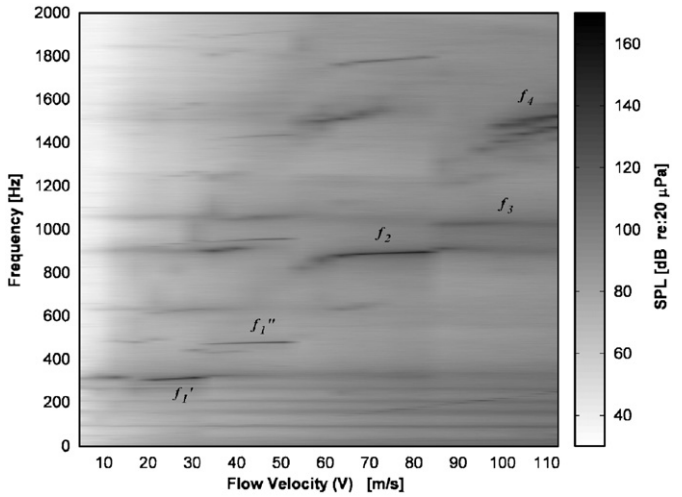

Fig. 15. Sound pressure level in dB of unchanged branch length for $\Delta L/L_{1,2} = 42\%$.

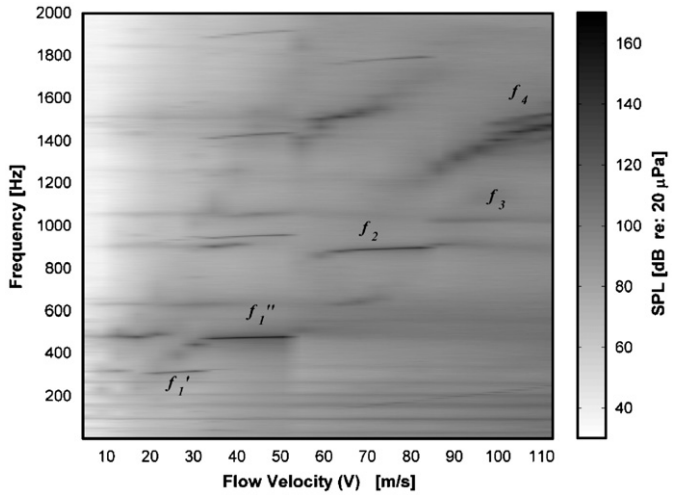

Fig. 16. Sound pressure level in dB of shortened branch for $\Delta L/L_{1,2} = 42\%$.

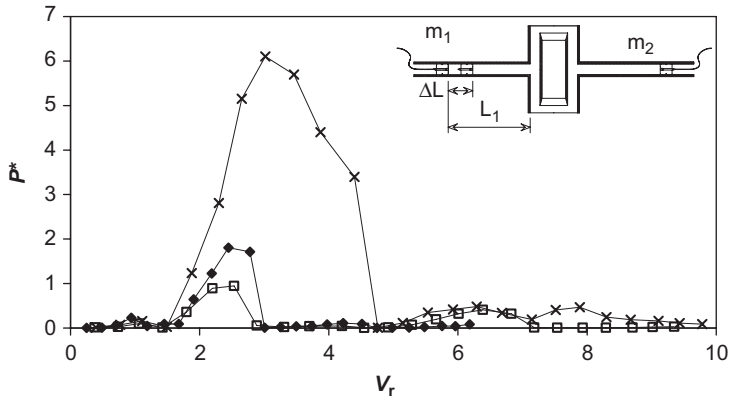

Fig. 17. Dimensionless amplitude response of shortened and unchanged branches, in comparison to baseline configuration. $\times$, $\Delta L/L_1 = 0\%$; $\blacklozenge$, $\Delta L/L_1 = 42\%$ shortened branch, $f_1'' = 476\,\text{Hz}$; $+$, $\Delta L/L_1 = 42\%$ unchanged branch $f_1' = 310\,\text{Hz}$.

Table 3
Comparison of d/D and D/λ used in this investigation to values of previous studies

Geometry	Ziada and Shine (1999)	Ziada and Bühlmann (1992)	Graf and Ziada (1992)	Present study
d/D	0.13, 0.25, 0.57	0.570	0.573	0.250
D/λ	0.073, 0.040, 0.028	0.0109, 0.021, 0.034	0.031	0.135

Table 4
Simulated and measured frequency of the first acoustic mode of the system for varying branch offsets

	Numerical simulations		Measured results	
	f_1'	f_1''	f_1'	f_1''
$\Delta L/L_{1,2} = 14.3\%$	309.7	354.6	313	359
$\Delta L/L_{1,2} = 28.6\%$	309.9	387.1	315	395
$\Delta L/L_{1,2} = 42.9\%$	310.5	469.3	316	478

In a previous study by Ziada and Bühlmann (1992), the effect of branch offset was investigated for the case of two tandem branches. It was found that an offset ratio of $\Delta L/L_{1,2} = 15\%$ produced reductions in the overall SPL by more than an order of magnitude. Graf and Ziada (1992) presented similar findings for coaxial branches, with approximately one order of magnitude reduction in maximum acoustic amplitude for an offset ratio of $\Delta L/L_{1,2} = 8\%$. In the present investigation, the first modes of detuned branches resonated independently of each other and over different ranges of flow velocity. The reduction in the resonance intensity was not as much as that observed in the above-mentioned studies. This disparity in behavior must be caused by differences in the diameter ratio (d/D) as well as in the branch length ratio ($L_{1,2}/D$). The latter is better expressed in terms of the ratio between the main pipe diameter and the acoustic wavelength (D/λ). Table 3 compares the main geometrical parameters of the present and previous experiments. As mentioned earlier, branches with smaller diameter ratio, as in the present geometry, have smaller radiation losses into the main duct. In addition, the acoustic response of each branch seems to become more independent of the other branch as the distance between their open ends becomes a larger fraction of the wavelength, i.e. higher D/λ. This supposition is supported by the finding that the detuned branches resonate at different frequencies and also that these frequencies are well predicted by considering each branch separately, as discussed in relation to Eq. (5).

The numerical simulation yielded accurate frequency prediction (within 2%) for the test cases with branch offset, predicting two independent acoustic modes corresponding to each different branch length. The results from a variety of these simulations can be found in Table 4.

6. Effect of annular flow thickness

One of the main distinctions between the geometry of the present study and other geometries studied in the literature is the presence of the inner cylinder to form an annular duct with coaxial branches. Experiments were conducted to determine the effect of the annular duct thickness, h, on the acoustic response of the system. This was accomplished by performing tests on several inner cylinders with different outer diameters. Different cases are identified by the ratio between annular duct thickness and branch diameter, h/d. Additional tests were also performed without inner cylinder, $D_i = 0$ and $h/d = 2$, for comparison with existing literature. Table 5 shows the dimensions of all cases tested.

Fig. 18 shows the frequency and dimensionless amplitude of the acoustic response of coaxial branches as functions of reduced velocity. Different symbols correspond to various values of the ratio h/d. It is clear that the thickness of the annular duct, relative to the duct diameter, does not have a strong influence on the acoustic response of the system. For example, the response of the first acoustic mode is almost identical in all cases with inner cylinders of different diameters. However, the case *without* an inner cylinder has significantly higher pressure pulsations for the first acoustic mode than all other cases. The maximum values of dimensionless pressure for all cases, both with and without an inner cylinder, occur at a reduced velocity of $V_r \approx 3.0$.

Table 5
Different inner cylinder sizes tested and the corresponding ratio of h/d

Annulus outer diameter D_i (mm)	h/d
0	2
38.1	1.5
76.2	1
114.3	0.5

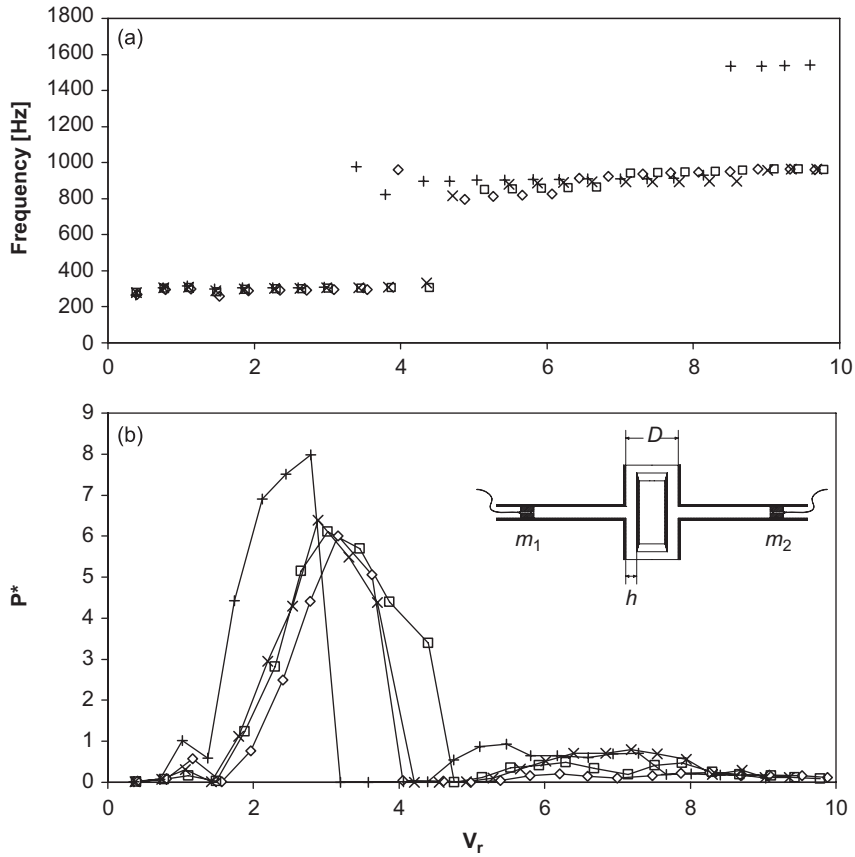

Fig. 18. Frequency response and acoustic pressure of duct with varying sizes of inner cylinder: +, $h/d = 2.0$ (*no inner cylinder*); ×, $h/d = 1.5$; □, $h/d = 1.0$; ◇, $h/d = 0.5$.

The frequency response of all cases with varying h/d ratios is shown at the top of Fig. 18. It can be seen that the overall frequency response of all the cases is quite similar. All acoustic modes are of approximately the same frequency, and are excited at roughly the same flow velocity in the main pipe. The only exception is for the case without inner cylinder, which tends to promote a higher acoustic mode, the fourth mode near 1500 Hz, at a lower reduced velocity.

7. Effect of splitter plates

In order to alleviate the intensity of acoustic resonances, especially those of the first mode, splitter plates were implemented in the annular duct. As shown in Fig. 5, the plates extended along the length of the annular duct and were

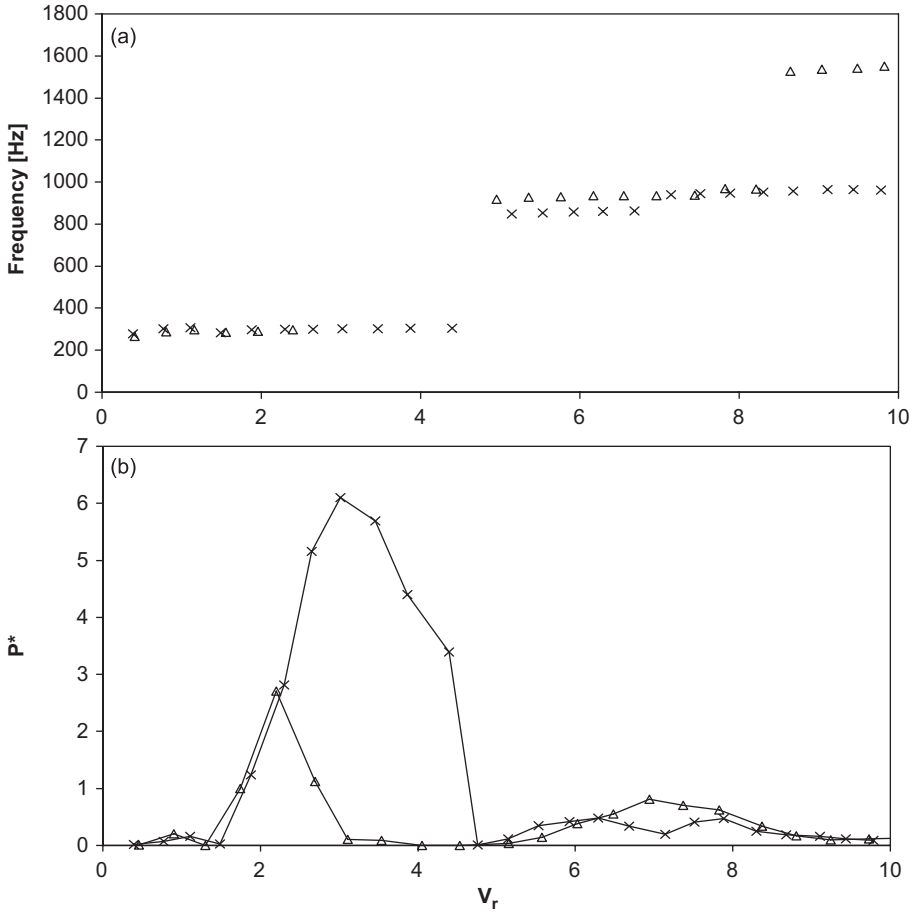

Fig. 19. Frequency response and dimensionless acoustic pressure of the duct with and without splitter plates: ×, no splitter plates; Δ, with splitter plate. $h/d = 1.0$ for both cases.

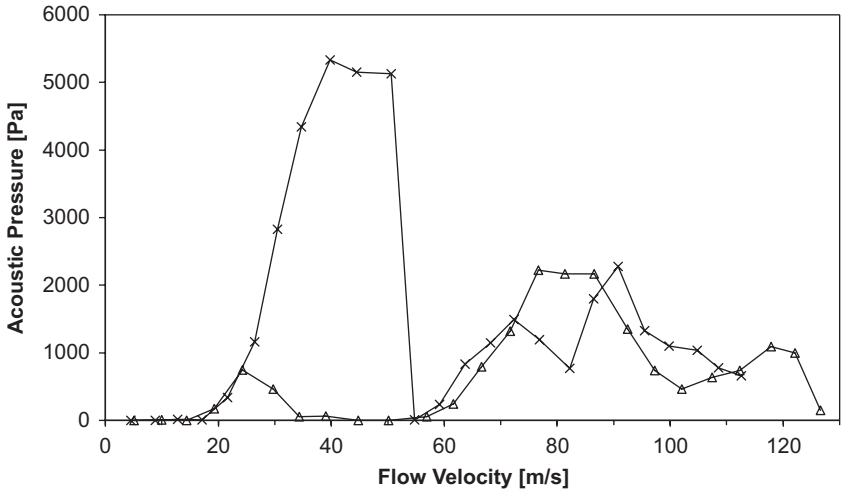

Fig. 20. Acoustic pressure of the duct with and without splitter plates: ×, no splitter plates; Δ, with splitter plate. $h/d = 1.0$ for both cases.

perpendicular to the axis of the branches, joining the inner cylinder with the outer cylinder forming the main duct. Care was taken to ensure an airtight seal between the duct surfaces and the splitter plates to eliminate the possibility of acoustic leakage, which may influence the acoustic response. The experiment was carried out using a configuration similar to the baseline configuration ($h/d = 1.0$), but with the splitter plates installed in the section.

The purpose of the splitter plates was to attenuate the first acoustic mode by de-coupling the two branches and attempting to weaken their interaction. In addition, the splitter plates would increase acoustic radiation into the main duct by imposing a greater portion of the acoustic standing wave in the main duct.

Fig. 19 shows the frequency and the dimensionless amplitude of the acoustic pressure versus reduced velocity for the cases with and without the splitter plates present. Regarding the effect of the splitter plates on the frequency of the acoustic modes, Fig. 19(a) shows that the plates reduce the frequency for the first acoustic mode by approximately 15 Hz, indicating that the standing acoustic wave is migrating around the plates as it was intended. Thus, the splitter plates have the effect of increasing the effective length between the branches and thereby reducing the resonance intensity of the first mode as can be seen in Fig. 19(b). Another effect which can be observed from Fig. 19(a) is that mode f_2 was not excited when the plates were present. Given that both the first and second acoustic modes of the duct, f_1 and f_2, have been suppressed or eliminated and the third and forth acoustic modes, f_3 and f_4, have been enhanced, the splitter plates seem to weaken the resonance of anti-symmetric acoustic modes (f_1 and f_2) and to enhance the response of symmetric acoustic modes (f_3 and f_4).

It appears from the results of Fig. 19(b) that the splitter plates have not been particularly effective in the reduction of the acoustic pulsations, reducing the dimensionless pressure by a factor of two only for the first acoustic mode of the duct. However, the actual acoustic pressure versus flow velocity in the main pipe, which is plotted in Fig. 20, shows a significant reduction in the amplitude of the first acoustic mode. The apparent discrepancy between the results of the two figures is due to the lower resonant frequency of the first acoustic mode for the case with splitter plates installed. The lower frequency of this mode is excited at a lower flow velocity, and thus a lower dynamic pressure, which results in a higher dimensionless pressure for this mode. The splitter plates have enhanced the response of higher modes for flow velocities exceeding 60 m/s; however, the splitter plates have shown to be effective in attenuating significant acoustic pressures for a range of flow velocities up to ~55 m/s.

8. Summary and conclusions

The aeroacoustic response of an annular duct with coaxial side-branches was examined. The duct was found to excite several acoustic modes, the strongest in all cases being the first acoustic mode, consisting of $\frac{1}{4}$ acoustic wavelength (λ) along each branch. The measured frequency of first acoustic mode was not well predicted by assuming the length between the ends of the branches to be equivalent to $\frac{1}{2}\lambda$. A numerical study was performed to determine the effects of diameter ratio and branch length ratio on the frequency of the first acoustic mode. This study showed that both length and diameter ratios have strong effects on the resonance frequencies of relatively short branches, e.g. for $L_{1,2}/D < 5$. For these short branches, the experimental and simulation results suggest that the frequency of the first mode can be accurately predicted from the expression for single side-branches.

The effect of the annular flow thickness was investigated both experimentally and numerically. The numerical simulation showed that the annular flow thickness ratio (h/d) does not affect the first mode frequency for the range tested. The acoustic pressure without the inner cylinder however, in comparison to that with the inner cylinder present, was about 20% larger for the first mode.

Several passive countermeasures were tested to evaluate their effectiveness. First, detuning the branches was considered. Even for relatively small offsets in branch lengths, two distinct tones were developed corresponding to the branch different lengths. The acoustic sound pressure of these tones was still quite significant, up to 50% of the tones generated for well-tuned branches. The effect of two splitter plates positioned in the annular duct was also investigated. These plates were shown to be effective in suppressing the first acoustic mode of the duct, as other antisymmetric acoustic modes. Installing the plates in the main pipe reduced the intensity of acoustic resonance for flow velocities up to ~55 m/s. However, the splitter plates did have the effect of enhancing the response of the symmetric acoustic modes, which were excited at high flow velocities.

The present results suggest that when short branches with small diameter ratio are acoustically decoupled, by means of branch length detuning, they behave as independent acoustic resonators. This was particularly evident when the detuned branches produced two distinct resonant tones of different amplitudes. The quality of small, short branches to produce independent tones explains why the tested attenuation techniques were not as effective as in previous studies dealing with longer and larger diameter side-branches.

Acknowledgments

The authors would like to thank Dr Francois Moyroud from Rolls-Royce Defense Aerospace in Bristol, England, for his constructive comments and keen interest in this study.

References

Baldwin, R.M., Simmons, H.R., 1986. Flow-induced vibration in safety relief valves. ASME Journal of Pressure Vessel Technology 108, 267–272.

Bravo, R., Ziada, S., Dokainish, M., 2004. Aeroacoustic response of an annular duct with coaxial side branches. In: Proceedings of the 11th AIAA/CEAS Aeroacoustics Conference (26th AIAA Aeroacoustics Conference), Monterrey, CA, May 2005.

Bruggeman, J.C., Hirschberg, A., Van Dongen, M.E.H., Wijnands, A.P.J., Gorter, J., 1991. Self-sustained aero-acoustic pulsations in gas transport systems: experimental study of the influence of closed side branches. Journal of Sound and Vibration 150, 371–393.

Chen, Y.N., Florjancic, D., 1975. Vortex-induced resonance in a pipe system due to branching. In: Proceedings of International Conference on Vibration and Noise in Pump, Fan and Compressor Installations, University of Southampton, England, pp. 79–86.

Chen, Y.N., Stürchler, R., 1977. Flow-induced vibrations and noise in a pipe system with blind branches due to coupling of vortex shedding. Internoise 77, B189–B203 Zürich.

DeBoo, G., Ramsden, K., Gesior, R., Strub, B., 2007. Identification of quad-cities main steam line acoustic sources and vibration reduction. In: Proceedings of PVP 2007, 2007 ASME Pressure Vessels and Piping Division Conference, pp. 1–7.

Gillessen, R., Roller, R., 1989. Verminderung und besietigung von schwingungen an rohrleitungssystemen (Reduction and elimination of vibration of piping systems). In: ''Minderung von Rohrleitungsschwingungen,'' VDI Berichte vol. 748, pp. 195–222.

Graf, H.R., Ziada, S., 1992. Flow induced acoustic resonance in closed side branches: an experimental determination of the excitation source. In: Proceedings of the Third International Symposium on Flow-Induced Vibration and Noise, vol. 7, ASME WAM, Anaheim, pp. 63–80.

Howe, M.S., 1975. Contributions to the theory of aerodynamic sound, with application to excess jet noise and the theory of the flute. Journal of Fluid Mechanics 71, 625–673.

Kinsler, L.E., Frey, A.E., Coppens, A.B., Sanders, J.V., 2000. Fundamentals of Acoustics. Wiley.

Michalke, A., 1965. On spatially growing disturbances in an inviscid shear layer. Journal of Fluid Mechanics 23, 521–544.

NRC Information Notice 2002–26, Supplement 1, 2002. Additional failure of steam dryer cover plate after a recent power uprate, US Nuclear Regulatory Commission, Washington, DC.

Ziada, S., 1993. Flow-excited resonances of piping systems containing side-branches: excitation mechanism counter-measures and design guidelines. International Seminar on Acoustic Pulsations in Rotating Machinery, AECL CANDU, Mississauga, Canada, pp. 1–34.

Ziada, S., 1994. A flow visualisation study of flow-acoustic coupling at the mouth of a resonant side-branch. Journal of Fluids and Structures 8, 391–416.

Ziada, S., Bühlmann, E.T., 1992. Self-excited resonances of two side-branches in close proximity. Journal of Fluids and Structures 6, 583–601.

Ziada, S., Shine, S., 1999. Strouhal numbers of flow-excited acoustic resonance of closed side branches. Journal of Fluids and Structures 13, 127–142.